ELSEVIER

Journal of Fluids and Structures 25 (2009) 1021–1028

JOURNAL OF FLUIDS AND STRUCTURES

www.elsevier.com/locate/jfs

Brief Communication

# Passive control of wake flow by two small control cylinders at Reynolds number 80

C.-H. Kuo*, C.-C. Chen

*Department of Mechanical Engineering, National Chung Hsing University, No. 250 Kuo-Kuang Road, Taichung 40227, Taiwan*

Received 6 April 2008; accepted 15 May 2009
Available online 8 July 2009

**Abstract**

Passive control of the wake behind a circular cylinder in uniform flow is studied by numerical simulation at $Re_D = 80$. Two small control cylinders are placed symmetrically along the separating shear layers at various stream locations. In the present study, the detailed flow mechanisms that lead to a significant reduction in the fluctuating lift but maintain the shedding vortex street are clearly revealed. When the stream locations lie within $0.8 \leq X_C/D \leq 3.0$, the alternate shedding vortex street remains behind the control cylinders. In this case, the symmetric standing eddies immediately behind the main cylinder and the downstream delay of the shedding vortex street are the two primary mechanisms that lead to a 70–80% reduction of the fluctuating lift on the main cylinder. Furthermore, the total drag of all the cylinders still has a maximum 5% reduction. This benefit is primarily attributed to the significant reduction of the pressure drag on the main cylinder. Within $X_C/D > 3.0$, the symmetry of the standing eddy breaks down and the staggered vortex street is similar to that behind a single cylinder at the same Reynolds number. In the latter case, the mean pressure drag and the fluctuating lift coefficients on the main cylinder will recover to the values of a single cylinder.


*Keywords:* Passive wake control; Lift and drag reduction; Vortex shedding

## 1. Introduction

Because of the diversified flow phenomena for a wide range of Reynolds numbers, the wake flows behind bluff bodies in uniform flow have attracted the interest of a large number of investigators using either numerical or experimental methods. The wake flow patterns are strong functions of the Reynolds number, turbulence intensity, aspect ratio, blockage ratio, end effects and wall proximity. Details of the circular cylinders in uniform flow can be found in a book by Zdravkovich (1997, 2003). There are active and passive methods to manipulate the wake flows behind circular cylinders (Kuo et al., 2007). The main objectives to manipulate the wake flows are: (i) to reduce the form drag (Tokumaru and Dimotakis, 1991), (ii) to suppress vortex shedding (Strykowski and Sreenivasan, 1990; Lecordier et al., 1991) and (iii) to change the heat transfer characteristics (Igarashi, 1998; Lange et al., 1998).

Fig. 5 of Strykowski and Sreenivasan (1990) showed that if the small control cylinder is placed within a defined region in the near-wake of the main cylinder, the wake behind the main cylinder could be suppressed effectively at a Reynolds

*Corresponding author. Tel.: +886 422840433x314; fax: +886 422877170.
*E-mail address:* chkuo@dragon.nchu.edu.tw (C.-H. Kuo).

0889-9746/$ - see front matter 
doi:10.1016/j.jfluidstructs.2009.05.007

**Nomenclature**

| | |
|---|---|
| $\bar{C}_{Dp}$ | pressure drag coefficient, $\bar{C}_{Dp} = \int \bar{C}_{px}(\theta) D\, d\theta/2A$ |
| $\bar{C}_{Df}$ | frictional drag coefficient, $\bar{C}_{Dt} - \bar{C}_{Dp}$ |
| $\bar{C}_{Dt}$ | total drag coefficient |
| $\langle C_L \rangle$ | fluctuating lift coefficient, $\langle C_L \rangle = \int \bar{C}_{py}(\theta) D\, d\theta/2A$ |
| $\bar{C}_p$ | fluctuating surface pressure coefficient, $\bar{C}_p(\theta) = \bar{p}(\theta)/(\frac{1}{2}\rho U_i^2)$ |
| $D$ | diameter of main cylinder (cm) |
| $d$ | diameter of control cylinder, $d/D = 1/4$ |
| $\ell_v$ | vortex formation length (cm) |
| $\mathrm{Re}_D$ | Reynolds number, $\mathrm{Re}_D = \rho U_i D/\mu$ |
| $\mathrm{St}_D$ | Strouhal number, $\mathrm{St}_D = fD/U_i$ |
| S1, S2, S3 | saddle points in the flow field |
| $t$ | time instant (s) |
| $U_i$ | uniform inflow speed (cm/s) |
| $x$, $y$, $z$ | streamwise, transverse and spanwise coordinates |
| $X_C$, $Y_C$ | location of the control cylinders |
| $\theta$ | angle from the forward stagnation point of the main cylinder (degree) |
| $\mu$ | viscosity (dyn-s/cm$^2$) |
| $\rho$ | density (g/cm$^3$) |

*Subscript*

| | |
|---|---|
| $o$ | refers to the condition without control cylinders |

*Superscript*

| | |
|---|---|
| * | refers to nondimensional quantities |

number of 80. Suppression of the vortex street is associated with damping of the absolute instability in the near-wake region. They also showed that wake suppression is the most efficient when the small control cylinder is placed near the centre of this contoured region. In terms of the velocity spectrum, the spectral peak is predominant if the small control cylinder is placed outside this identified region. The spectral peak gradually becomes broadband and is finally diminished as the control cylinder is moved vertically from the outside to the centre of this region. Their experimental and numerical results also indicate that the domain of this region strongly depends on the Reynolds number as well as the diameter ratio. For the Reynolds number effect (from 80 to 300), a recent study by Kuo et al. (2007) showed the detailed flow structures and revealed the primary mechanism that led to significant lift and drag reduction without completely suppressing the shedding vortex street. For some low Reynolds number applications in microsystems, the cylinder is expected to have minimal drag and lift, but it still preserves the vortex street for mixing purposes. Concerning the control cylinders located outside the specified contoured region, the details of the flow structures are insufficient and the related mechanism leading to drag and lift reduction is not yet clear. Therefore, the objective of this study is to elucidate the flow structures from different control cylinders stream locations and the related mechanisms that lead to a reduction in the fluctuating lift and mean pressure drag on the main cylinder.

## 2. Flow system, conditions and CFD model validations

The flow domain and the boundary conditions of the corresponding physical system can be found in Fig. 1 of Kuo et al. (2007). The origin is defined at the centre of the main cylinder with diameter $D$. The centres of the control cylinders are located at ($X_C$, $\pm Y_C$). Two small control cylinders, having diameter ratio $d/D = 1/4$, are placed symmetrically along $Y_C/D = \pm 0.5$ at various stream locations (e.g., $X_C/D = 0.8$–$4.5$). The uniform flow enters the left boundary with a constant velocity $U_i$. The upper and the lower boundaries are located far from the main cylinder at $y/D = \pm 25$. The leftmost and the rightmost boundaries of the flow domain in Fig. 1 (Kuo et al., 2007) are located at $x/D = -10$ and 40, respectively. Further extension of the flow domain in both the $x$ and $y$ directions yields the same velocity and surface pressure distributions, and the maximum uncertainties of the free stream velocity and stagnation pressure coefficient are about 0.21% and 1.27%, respectively.

### 2.1. Navier–Stokes solver

The flow is assumed to be two-dimensional, unsteady, laminar and incompressible with constant properties. The force of gravity is excluded. Computations of the continuity and Navier–Stokes equations are carried out by the Fluent (2006) solver based on the finite volume method with quadrilateral differential control volumes (CV). The convective flux and diffusive flux terms are evaluated using the third-order Quick scheme and the second-order central differencing

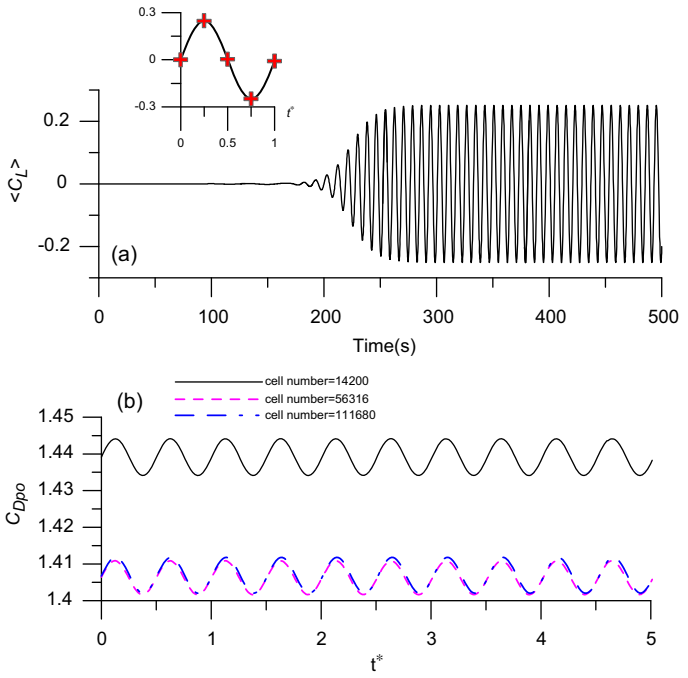


Fig. 1. (a) Time history of $\langle C_L \rangle$ during simulation process. (b) Periodic variations of $C_{Dpo}$ within the stable stage for three different mesh densities.

Table 1
Comparisons of the simulated data with those in the literature for a single circular cylinder at $\mathrm{Re}_D = 80$.

| Author | Strykowski and Sreenivasan (1990) | Zhou and Antonia (1992) | Norberg (2003) (experiments) | Williamson and Brown (1998) (experiments) | Henderson (1997) (numerical) | Present study (numerical) |
|---|---|---|---|---|---|---|
| $\mathrm{Re}_D$ | 80 | $<160$ | 80 | 80 | 80 | 80 |
| $\tilde{C}_{Dfo}$ | | | | | | 0.37 |
| $\tilde{C}_{Dpo}$ | | | | | | 1.405 |
| $\mathrm{St}_D$ | 0.18 | | 0.152 | 0.153 | 0.155 | 0.158 |
| $\langle C_L \rangle$ | | | 0.16 | | | 0.26 |
| $U_{\mathrm{conv}}$ | | $0.85U_i$ | | | | $0.88U_i$ |
| $\tilde{u}_{\mathrm{r.m.s}}$ | $0.2U_i$ at $y/D = 0.7$ | | | | | $0.27U_i$ at $y/D = 0.5$ |
| $fD^2/v$ | 12.5 | | 12.15 | | | 12.48 |

scheme, respectively. Moreover, the pressure–velocity coupling is calculated by the pressure implicit splitting of operator (PISO) algorithm. The iteration process stops when the sum of the absolute residuals for all variables is less than $10^{-4}$. In addition, the flow domain is divided into several blocks with different mesh densities to satisfy the local spatial resolution in the flow field of the large velocity gradient.

### 2.2. Validation of CFD simulation model

For a circular cylinder in uniform flow, the results obtained by the present model are listed in Table 1 for comparison with the experimental data of Norberg (2003) at the same Reynolds number. Comparisons between the maximum value of $\tilde{u}_{\mathrm{r.m.s.}}$, the convective speed $U_{\mathrm{conv}}$ and the Strouhal number are also provided. In general, they agree very well with those presented in the literature. A large deviation in $\langle C_L \rangle$ is found because the present simulation is purely

two-dimensional, whereas that in Norberg (2003) is three-dimensional. Fig. 1(a,b) shows the entire time history of $\langle C_L \rangle$ and $C_{Dpo}$ for several cycles selected from the stable state. It is evident that the results of $\langle C_L \rangle$ are insensitive to the cell numbers, whereas the smallest cell number will lead to a large deviation of $C_{Dpo}$. Based on these preliminary results, this computational fluid dynamics (CFD) simulation model will be employed to study the wake flow structures modified by two small control cylinders situated symmetrically about the wake centreline. In this study, a large cell number ($4.5 \times 10^5$–$1.7 \times 10^6$) is employed for all cases to ensure that the results will be grid-independent.

## 3. Results and discussion

### 3.1. Near-wake flow structures

In Fig. 2, the enlarged views of detailed velocity vectors and the associated streamline patterns in the immediate near-wake region of the main cylinder are illustrated when the control cylinders are located at $X_C/D = 1.3$ and 2.5. Within

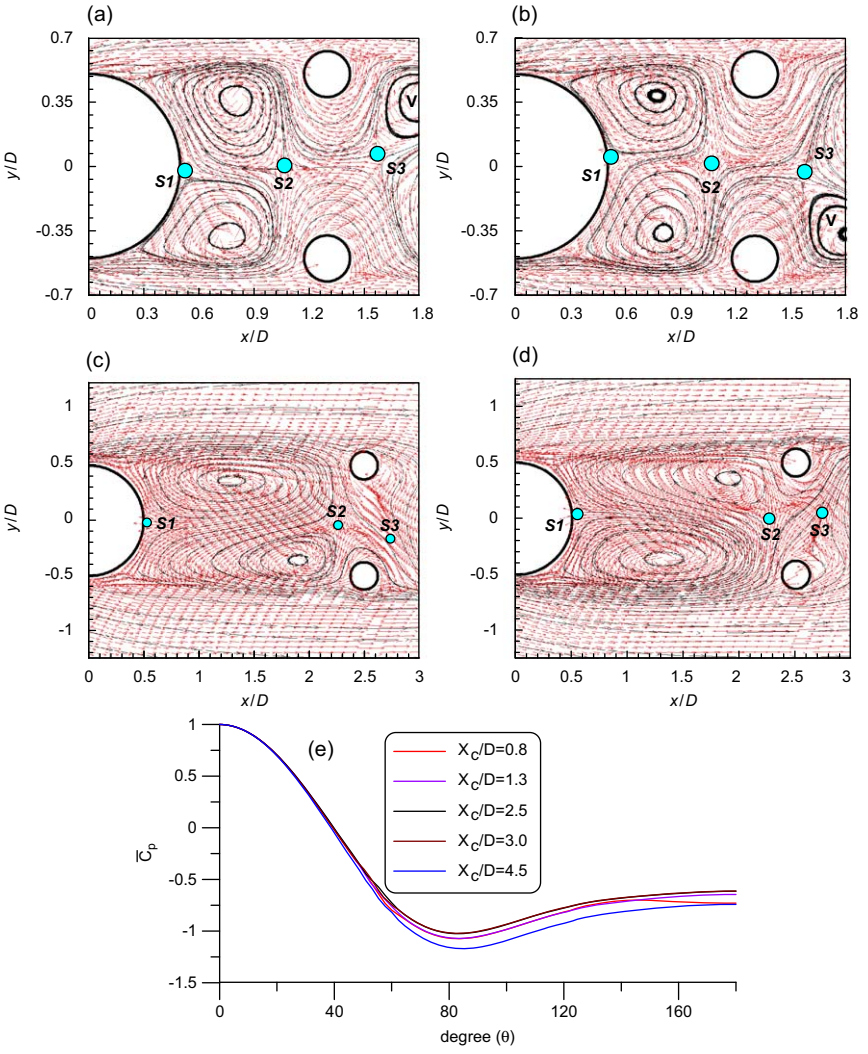


Fig. 2. (a–d) Velocity vectors and the associated streamlines between the main and the control cylinders at $X_C/D = 1.3$ and 2.5 for $\mathrm{Re}_D = 80$. Two instants, $t^* = \frac{1}{4}$ and $t^* = \frac{3}{4}$, are selected at which the fluctuating lift force on the main cylinder attains the maximum and minimum, respectively. (e) The distributions of the mean pressure coefficient on the cylinder surface for various locations of the control cylinder ($X_C/D$) from 0.8 to 4.5 at $\mathrm{Re}_D = 80$. (a) $X_C/D = 1.3$, $t^* = \frac{1}{4}$; (b) $X_C/D = 1.3$, $t^* = \frac{3}{4}$; (c) $X_C/D = 2.5$, $t^* = \frac{1}{4}$; and (d) $X_C/D = 2.5$, $t^* = \frac{3}{4}$.

the shedding cycle, two instants ($t^* = \frac{1}{4}$ and $\frac{3}{4}$) with opposite phases are selected to reveal the stationary eddy characteristics in this region. In Fig. 2(a,b), when the control cylinders are located at $X_C/D = 1.3$, the locations of the saddle points S1 and S3 remain nearly unchanged. The three-way saddle point S1 (solid circle) denotes the instantaneous stagnation point on the rear surface of the main cylinder. The four-way saddle point, S3, exists in the flow region just beyond the control cylinders. In addition, an extra four-way saddle point S2 appears to be situated between S1 and S3. Two standing eddies are formed and are symmetric about the wake centreline. Though the vortex street sheds alternately behind the control cylinders, the symmetric eddies remain stationary within the shedding cycle. The symmetric flow structure of symmetric stationary eddies continues to exist for the cases of $X_C/D = 1.0$–$2.0$. It is not until $X_C/D = 2.5$ that the symmetric flow structure breaks down. However, these eddies move only slightly in the streamwise direction without shedding downstream (Fig. 2(c,d)). Finally, the vortex street forms in this gap region between the main and the control cylinders and starts to shed alternately downstream for $X_C/D \geq 4.5$. In Fig. 2(e), the mean pressure coefficients are plotted to illustrate the influence of the control cylinder at different locations. Along the frontal surface, all the $\bar{C}_p$ distributions are nearly equal; they start to deviate from $\theta = 60^\circ$ toward the rear surface. Along the rear surface, the distribution is the lowest for $X_C/D = 4.5$ and the highest for $X_C/D = 3.0$, implying that the value of $\bar{C}_{Dp}$ will reach a maximum and a minimum at $X_C/D = 4.5$ and 3.0, respectively.

### 3.2. Lift and drag variations

The fluctuating lift and the mean pressure drag coefficients, $\langle C_L \rangle$ and $\bar{C}_{Dp}$, on the main cylinder are shown in Fig. 3(a) as functions of the locations of the control cylinders. Note that both quantities are normalized by their counterparts, $\langle C_{Lo} \rangle$ and $\bar{C}_{Dpo}$, of a single cylinder at the same Reynolds number. The magnitudes of $\langle C_L \rangle$ remain significantly small in the region $0.8 \leq X_C/D \leq 3.0$. In the region between $X_C/D = 3.0$ and 3.5, the magnitudes of $\langle C_L \rangle$ and $\bar{C}_{Dp}$ experience sudden jumps. The alternate shedding vortex street is the main source leading to the fluctuating lift force on the main cylinder. Furthermore, the magnitudes of the fluctuating surface pressure, induced by the shedding vortex street, strongly depend on the strength and vortex formation length of the shedding vortex. In Fig. 3(a), the

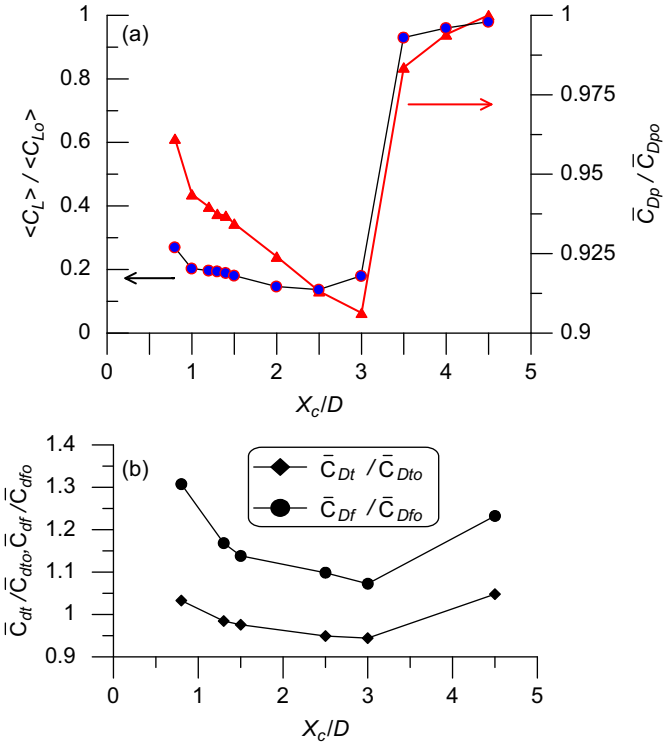


Fig. 3. (a) Variations of the fluctuating lift and mean pressure drag coefficients; (b) variations of the total drag and friction drag coefficients as $X_C/D$ ranges from 0.8 to 4.5 at $\mathrm{Re}_D = 80$. Note that all the coefficients are normalized by $\langle C_{Lo} \rangle$, $\bar{C}_{Dpo}$ and $\bar{C}_{Dyo}$, $\bar{C}_{Dfo}$, respectively.

sudden jump in $\langle C_L \rangle$ is caused by two primary factors. The first is the presence of two symmetric standing eddies in the region between the main and the control cylinder. The second is the downstream delay of the shedding vortex street behind the control cylinders. The closer the vortex formation to the main cylinder, the larger the amplitude of the fluctuating lift or pressure. In Fig. 3(a), the fluctuating lift and the mean pressure drag coefficients asymptotically approach that of a single cylinder at a large distance along the stream ($X_C/D \geq 4.5$).

Fig. 3(b) shows the ratios of the total and the frictional drag coefficients of all the cylinders (main and control cylinders) to those of a single cylinder as a function of $X_C/D$. The total drag is evaluated by the momentum balance in the direction along the stream on a finite control volume including all the cylinders. Similar variation trends of $\bar{C}_{Df}$ and $\bar{C}_{Dt}$ are evident in Fig. 3(b), except for the differences in the magnitude. In other words, the ratios decrease monotonically from $X_C/D = 0.8$ and reach a minimum value at $X_C/D = 3.0$. For the case of $X_C/D = 4.5$, both ratios increase again and are slightly higher than $\bar{C}_{Dto}$ and $\bar{C}_{Dfo}$. In Fig. 3(b), the ratio of $\bar{C}_{Df}/\bar{C}_{Dfo}$ is greater than 1.0, indicating that the friction drag always increases as long as the control cylinders are added in the flow field. On the other hand, the ratios of the total drag of all cylinders decrease monotonically and are smaller than 1.0 in the range $0.8 < X_C/D \leq 3.0$. At this Reynolds number, the friction drag is about 20% of the total drag on a single cylinder in uniform flow. Thus, the reduction of the total drag on all cylinders primarily benefits from the significant reduction of the pressure drag on the main cylinder (Fig. 3(a)).

### 3.3. Mechanism of wake modification and related lift alteration

The mean streamwise velocity, normalized by $U_i$, along the wake centreline ($y/D = 0$) is depicted in Fig. 4. Along the flow direction, there are four different flow regimes separated by points of zero velocity: the standing symmetric eddy (SE), the jet region (J), and the near-wake (NW) and the far-wake (FW) regions. In Fig. 4, the distance $\ell_v$ is defined as the vortex formation length. Along the flow direction, the centreline velocity $U_c^*$ experiences the negative values in the SE and NW regions, and becomes positive in the J and FW regions. All the locations of maximum positive $U_c^*$ in the J region correspond to the locations of the control cylinders (Kuo et al., 2007). However, the variations in the centreline

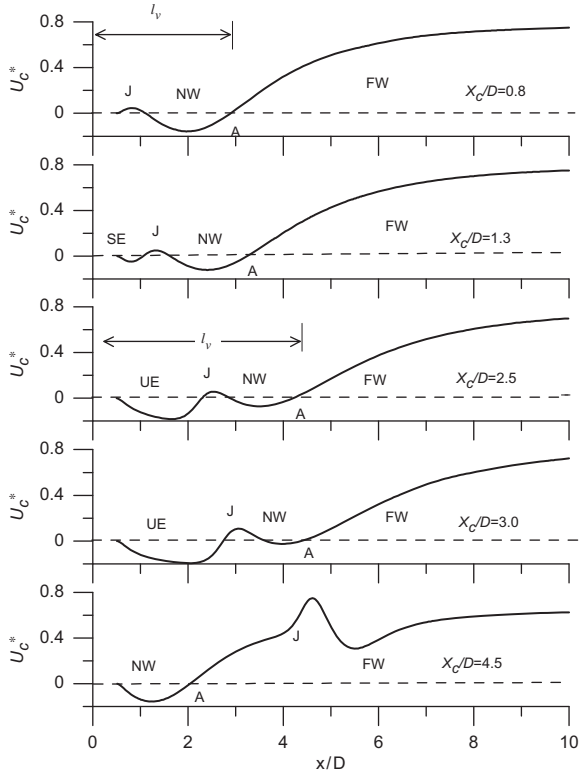


Fig. 4. Variations of the mean velocity along the wake centreline as $X_C/D$ changes from 0.8 to 4.5 at $\mathrm{Re}_D = 80$. Note that all the data points start from $x/D = 0.5$ where it corresponds to the rear stagnation point of the main cylinder.

Table 2
Variations of the Strouhal number and the vortex formation length as a function of $X_C/D$.

| $X_C/D$ | 0.8 | 1.3 | 1.5 | 2.5 | 3.0 | 3.5 | 4.5 |
|---|---|---|---|---|---|---|---|
| $St_D$ | 0.145 | 0.142 | 0.138 | 0.126 | 0.122 | 0.148 | 0.152 |
| $\ell_v/D$ | 3.0 | 3.2 | 3.5 | 4.2 | 4.6 | 2.5 | 2.1 |

velocity in the FW region are similar to those obtained by Sung and Yoo (2003). For $X_C/D = 0.8$–3.0, the extent of the nearly symmetric flow structure (SE or UE) along the stream is significantly enlarged, and the vortex formation length increases monotonically. Downstream from point A, the vortex street starts to shed into the far-wake region. The distance between point A and the origin clearly indicates the downstream delay of the shedding vortex street. In Table 2, it is demonstrated that the longer the vortex formation length, the smaller is the Strouhal number. The inverse relationship between the vortex formation length and the Strouhal number provides an additional link to the fact that the enlarged SE or UE region and the downstream delay of the shedding vortex street is associated with a lower shedding frequency.

## 4. Concluding remarks

The present numerical study reveals the wake flow structures behind a circular cylinder manipulated by two small control cylinders and elucidates the primary mechanism that leads to a reduction of the lift and the pressure drag on the main cylinder. Two small control cylinders, with diameter ratio $d/D = \frac{1}{4}$, are placed along two separating shear layers at various stream locations. The Reynolds number, based on the main cylinder diameter, is 80. When the control cylinders lie within $0.8 \leq X_C/D \leq 3.0$, the fluctuating lift on the main cylinder shows a 70–80% reduction without completely suppressing the vortex street. Addition of the control cylinders always increases the friction drag of all the cylinders. The total drag of all the cylinders still has a maximum 5% reduction. This benefit is primarily attributed to the significant reduction of the pressure drag on the main cylinder. The mechanism leading to significant reduction in the fluctuating lift is two-fold. The first is the formation of two symmetric standing eddies in the region between the main and two control cylinders. The second is the delay of the shedding of the vortex street behind the control cylinders. For $X_C/D > 3.0$, the symmetry of the standing eddy breaks down, and the vortex street starts to shed alternately downstream. Therefore, the mean pressure drag and the fluctuating lift coefficients on the main cylinder recover to those of a single cylinder.

## Acknowledgement

The authors are grateful for the project supported by the National Science Foundation of the Republic of China under the Grant no. NSC-90-2212-E-005-026.

## References

Fluent 6.2, 2006. User's Manual. Fluent Inc.

Henderson, R., 1997. Nonlinear dynamics and pattern formation in turbulent wake transition. Journal of Fluid Mechanics 352, 65–112.

Igarashi, T., 1998. Visualization of flow around a bluff body controlled by a rod set upstream. In: Carlomagno, G.M., Grant, I. (Eds.). The 8th International Symposium on Flow Visualization, Sorrento, Italy, pp. 101.1–101.6.

Kuo, C.H., Chiou, L.C., Chen, C.C., 2007. Wake flow pattern modified by small control cylinders at low Reynolds number. Journal of Fluids and Structures 23, 938–956.

Lange, C.F., Durst, F., Breuer, M., 1998. Momentum and heat transfer from cylinders in laminar cross flows at $10^{-4} \leq Re \leq 200$. International Journal of Heat and Mass Transfer 41, 3409–3430.

Lecordier, J.C., Hamma, L., Parantheon, P., 1991. The control vortex shedding behind heated cylinders at low Reynolds numbers. Experiments in Fluids 10, 224–229.

Norberg, C., 2003. Fluctuating lift on a circular cylinder: review and new measurement. Journal of Fluids and Structures 17, 57–96.

Strykowski, P.J., Sreenivasan, K.R., 1990. On the formation and suppression of vortex shedding at low Reynolds numbers. Journal of Fluid Mechanics 218, 71–107.

Sung, J., Yoo, J.Y., 2003. Near wake vortex motions behind a circular cylinder at low Reynolds number. Journal of Fluids and Structures 17, 261–274.

Tokumaru, P.T., Dimotakis, P.E., 1991. Rotary oscillation control of a cylinder wake. Journal of Fluid Mechanics 224, 77–90.

Williamson, C.H.K., Brown, G.L., 1998. A series in $1/\sqrt{\mathrm{Re}D}$ to represent the Strouhal–Reynolds number relationship of the cylinder wake. Journal of Fluids and Structures 12, 1073–1085.

Zdravkovich, M.M., 1997. Flow Around Circular Cylinders, vol. 1: Fundamentals. Oxford University Press, New York.

Zdravkovich, M.M., 2003. Flow Around Circular Cylinders: A Comprehensive Guide Through Flow Phenomena, Experiments, Applications, Mathematical Models, and Computer Simulations, vol. 2: Applications. Oxford University Press, New York.

Zhou, Y., Antonia, R.A., 1992. Convection velocity measurements in a cylinder wake. Experiments in Fluids 13, 63–70.